The Influence of Carbon and MoSi2 Addition on the Sinterability and Mechanical Properties of Titanium Boride (TiB2) Based Composites

Maria Sajdak , Kamil Kornaus * , Dariusz Zientara , Norbert Moskała , Sebastian Komarek , Kinga Momot , Edmund Golis , Łukasz Zych , Agnieszka Gubernat

Posted Date: 26 December 2023

doi: 10.20944/preprints202312.1989.v1

Keywords: Borides; UHTC; Hot Pressing; Silicides; Core-Shell

Article

The Influence of Carbon and $MoSi_2$ Addition on the Sinterability and Mechanical Properties of Titanium Boride (TiB_2) Based Composites

Maria Sajdak [1], Kamil Kornaus [1,*], Dariusz Zientara [1], Norbert Moskała [1], Sebastian Komarek [1], Kinga Momot [2], Edmund Golis [3], Łukasz Zych [1] and Agnieszka Gubernat [1]

[1] AGH University of Krakow, Faculty of Materials Science and Ceramics, Kraków, Poland
[2] Łukasiewicz Research Network, Krakow Institute of Technology, Kraków, Poland
[3] Jan Dlugosz University in Czestochowa, Częstochowa, Poland
* Correspondence: author: Kamil Kornaus PhD, kornaus@agh.edu.pl

Abstract: Titanium boride (TiB_2) is a material classified as ultra-high temperature ceramics. The TiB_2 structure is dominated by covalent bonds, which gives materials based on TiB_2 very good mechanical and thermal properties, but also makes them difficult to sinter. Obtaining dense TiB_2 polycrystals requires chemical or physical sintering activation. Carbon and molybdenum disilicide ($MoSi_2$) were chosen as sintering activation additives. Three series of samples were made, the first with carbon additives: 0 to 4 wt.%; the second with 2.5, 5 and 10 wt.%. $MoSi_2$ and the third with both additions of 2 wt.% carbon and 2.5, 5 and 10 wt.% $MoSi_2$. $MoSi_2$. On the basis of dilatometric sintering analysis, all additives were found to have a favourable effect on sinterability of TiB_2, and it was determined that sintering of TiB_2 with carbon addition can be carried at 2100°C and with $MoSi_2$ and both additives at 1800°C. The polycrystals were sintered using the hot pressing technique. On the basis of the studies conducted in this work, it was found that addition of 1 wt.% of carbon allows to obtain single-phase TiB_2 polycrystals of high density (>90%). The minimum $MoSi_2$ addition required to obtain dense sinters with a cermet-like microstructure was 5 wt.%. High density was also achieved by materials containing both additives. Samples with higher $MoSi_2$ content, i.e. 5 and 10% showed densities close to 100%. Mechanical properties such; as Young's modulus, hardness and fracture toughness (K_{Ic}) of the polycrystals and composites were similar for samples with densities exceeding 95%. The Vickers hardness was 23 to 27 GPa, the fracture toughness (K_{IC}) was 4 to 6 $MPa \cdot m^{0.5}$ and the Young's modulus was 480 to 540 GPa. The resulting TiB_2-based materials showed potential in high-temperature applications.

Keywords: borides; UHTC; hot pressing; silicides; core-shell

1. Introduction

Ceramic materials classified as ultra-high-temperature ceramics (UHTC) are characterised by high melting point, good mechanical properties also at high temperature and high oxidation resistance. As they are increasingly used, more demands are placed on them [1,2]. The group of materials classified as UHTC includes metal borides of the 4th group of the periodic table of chemical elements, i.e. TiB_2, ZrB_2 and HfB_2. These borides have very high melting points (approx. 3000°C), good thermal and electrical conductivity, high hardness, good mechanical properties and oxidation resistance. These valuable properties of AlB_2 – type borides are result of dominant covalent bonds present in their structure, which on the other hand has a negative effect on sinterability of boride ceramics [1–4].

Improved sinterability of boride ceramics is achieved by using sintering additives (sintering activators) such as; nitrides: TiN, AlN, Si_3N_4 or HfN [2,5–9], carbides: TaC, SiC, B_4C, TaC [2,10–15], silicides: $MoSi_2$, $TiSi_2$, $TaSi_2$ [4,16–23] or oxides: ZrO_2 [24–28]. The most commonly used sintering activators for boride ceramics including TiB_2 are $MoSi_2$ and SiC [2,4,13,15–17,21]. The effect of silicide additives on the sinterability and properties of TiB_2 was, among others, studied by Raju, Murthy et al [17,20]. With introduction of 2.5% $MoSi_2$ additive and the use of hot pressing technique the authors of the discussed papers obtained dense composites at 1700°C. According to the authors, $MoSi_2$

 doi:10.20944/preprints202312.1989.v1

removes oxide impurities and then deforms plastically due to high temperature, filling spaces between TiB_2 grains. In another paper, Murthy et al [4] investigated materials sintered by hot pressing with 0 to 25% $MoSi_2$ addition leading do samples with density close to 98%, grain size of 2-5 μm, high hardness of 25 – 27 GPa and fracture toughness of 5.1 $MPa \cdot m^{0.5}$. The optimum amount of $MoSi_2$ was 10% which resulted in fine-grained microstructure of the sinters and hardness of 27 GPa.

The paper presents results of studies on effect of carbon and $MoSi_2$ additives and effect of combined carbon and $MoSi_2$ additives on sinterability and mechanical properties of titanium diboride.

2. Materials and experimental procedure

The samples were prepared from the commercial powders: TiB_2, ABCR Company (GRADE F, cat.no. AB 134577), $MoSi_2$, Morton Thiokol (99%, cat.no. 48108). As a carbon precursor, phenol-formaldehyde resin of the NOVOLAK type (Organika Sarzyna, Poland) was used. During sintering it undergoes pyrolysis leaving 50 wt.% of amorphous carbon.

A reference sample of pure TiB_2 and three series of samples with various additives additions were made. The first series with addition of: 1%, 2%, 3% and 4% wt. carbon; the second with addition of: 2.5% , 5% and 10% wt. $MoSi_2$, and the third containing constant amount of 2% wt. of carbon and 2.5% , 5% or 10% wt. of $MoSi_2$. The sample denominations used in the work are summarised in Table 1.

Table 1. Denomiantion of the samples.

The initial composition	*Name*
TiB_2	TiB2_0
TiB_2+1%C	TiB2_1C
TiB_2+2%C	TiB2_2C
TiB_2+3%C	TiB2_3C
TiB_2+4%C	TiB2_4C
TiB_2+2.5%$MoSi_2$	TiB2_2.5MS
TiB_2+5%$MoSi_2$	TiB2_5.0MS
TiB_2+10%$MoSi_2$	TiB2_10MS
TiB_2+2%C+2.5%$MoSi_2$	TiB2_2C_2.5MS
TiB_2+2%C+5%$MoSi_2$	TiB2_2C_5.0MS
TiB_2+2%C+10%$MoSi_2$	TiB2_2C_10MS

The powder mixture components were weighted and then homogenised in ethanol in a ball mill for 12 h using SiC spherical grinding media. Then the alcohol was evaporated and the powders mixtures were granulated by passing through a nylon 6 sieve. Cylindrical samples with diameter 12 mm and height 3 – 4 mm were formed by an uniaxial double-ended pressing and then subjected to dilatometric analysis.

Dilatometric sintering analysis was performed in a high-temperature graphite dilatometer of the own construction. Sintering in the dilatometer was carried out in an argon flow with a heating rate 10°C/min. The end of sintering was an appearance of a characteristic *plateau* on a of linear dimensions change as a function of temperature. The dilatometric analysis made possible determination of the final temperature of the hot – pressing.

The granulated powders were hot–pressed in graphite dies in argon flow using Thermal Technology Inc. press.

 doi:10.20944/preprints202312.1989.v1

The reference sample and the samples with carbon addition were sintered at 25 MPa at 2100°C, and the samples with $MoSi_2$ and $MoSi_2$ and carbon addition were sintered at 25 MPa at 1800°C. All samples were kept at the final temperature for one hour. The heating rate in each case was 10°C/min.

Apparent density of the sintered samples was measured using the Archimedes method. The relative density was calculated using 4.52 g/cm^3 as the theoretical density of TiB_2. Surface of the samples was ground and polished using LaboPol (Struers) polishing machine. Their microstructure was analysed using Scios2 DualBeam (ThermoFisher) SEM microscope along with the EDS chemical analysis. In order to determine phase composition, XRD analysis was performed with the X'Pert Pro apparatus (PANanlitycal). The quantitative phase composition of the sinters was determined using the Rietveld method. Hardness measurements were carried out by the Vickers method using a FV-810 (Future-Tech) hardness tester. A standard load of 1 kg and an indenter pressing time of 10 seconds were used. The fracture toughness (K_{Ic}) was determined using the indentation method at 3 kg load of. The Niihara formula was used to calculate the critical stress intensity factor (K_{Ic}). Young's modulus measurements were carried out using the ultrasonic method by measuring velocity of transverse and longitudinal waves passing through the specimen using EPOCH 3 (Panametrics) ultrasonic defectoscope.

3. Results and discussion

3.1. Dilatometric analysis

Figure 1 shows dilatometric sintering (sample shrinkage vs. temperature) curves obtained for a series of samples with carbon addition and the reference sample. Sintering in the dilatometer was carried out up to 2150°C, and despite such high sintering temperature, sintering curves of the reference sample and the sample with 1 wt.% carbon addition do not show the *plateau* characteristic for the end of sintering.

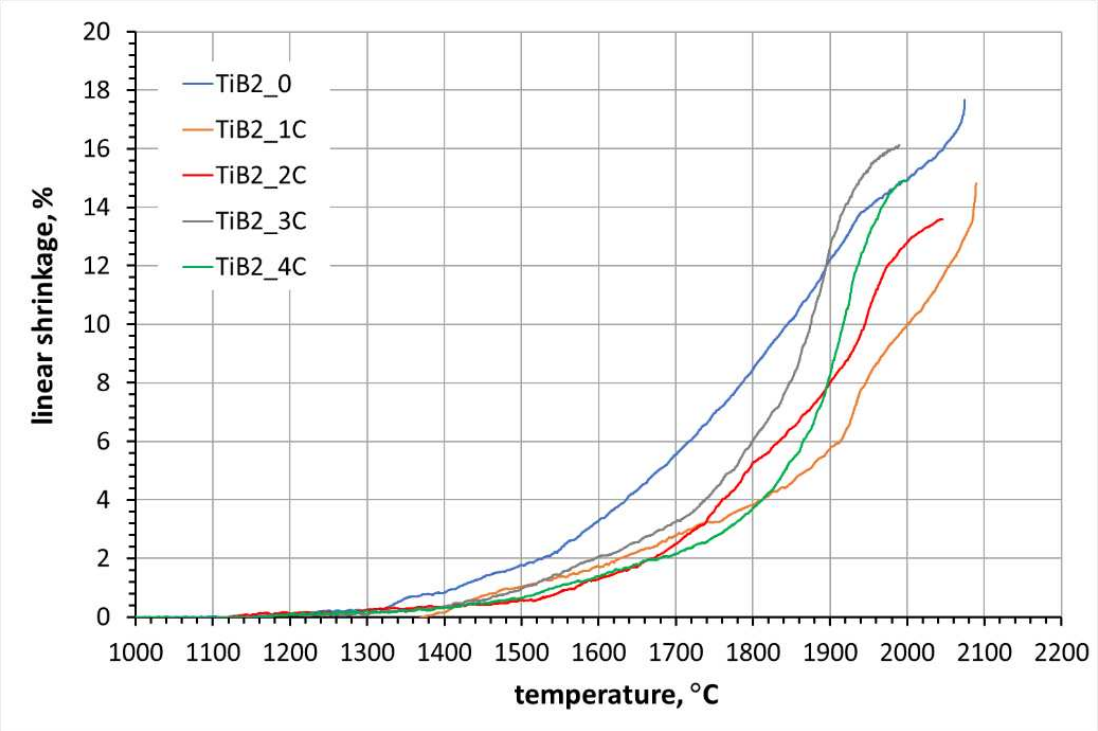

Figure 1. Dilatrometric sintering curves of the reference sample and samples with carbon addition.

A flattening of the sintering curve can be observed for samples with carbon addition higher than 1 wt.%. Sintering of samples with carbon additions between 2 and 4 wt.% ends at c.a. 2050°C.

Figure 2 presents the sintering curves of samples with $MoSi_2$ and $MoSi_2$ and carbon addition.

Preprints (www.preprints.org) | NOT PEER-REVIEWED | Posted: 26 December 2023 doi:10.20944/preprints202312.1989.v1

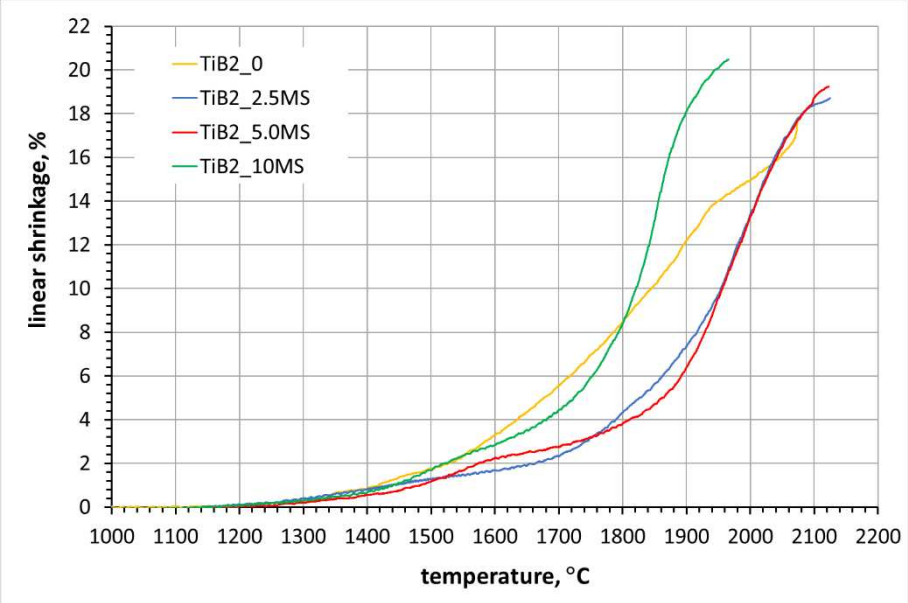

(**a**)

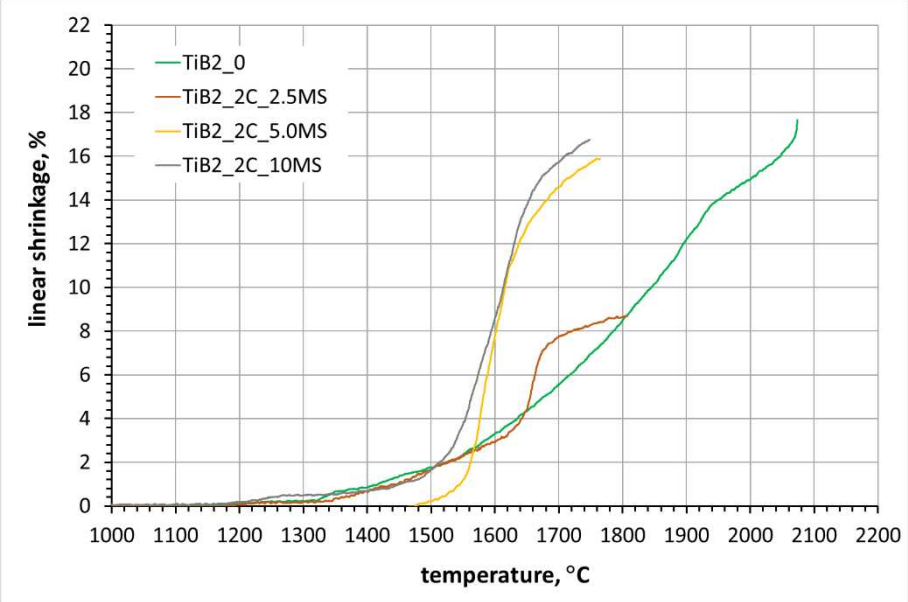

(**b**)

Figure 2. Dilatometric sintering curves of samples with: a) $MoSi_2$, b) carbon and $MoSi_2$ addition.

The course of curves of the samples with $MoSi_2$ indicate that this addition effectively activates TiB_2 sintering (Figure 2a). When the $MoSi_2$ additive is 2.5 and 5 wt.% the end of sintering occurs near 2100°C, while a significant reduction in sintering temperature occurs when the additive is 10 wt.% because then the temperature is close to 1950°C. The best sintering results gives the combination of carbon and $MoSi_2$ additives gives For samples containing 2 wt. % of carbon and 5 or 10 wt.% of $MoSi_2$ the characteristic *plateau* indicating the end of sintering occurs around 1700-1750°C. The sample containing 2 wt.% carbon and 2.5 wt.% $MoSi_2$ addition shows the lowest linear shrinkage ~ 8% and its sintering ends near 1800°C (Figure 2b). The beginning of sintering of the reference sample and the samples with carbon addition is in the range 1300 – 1400°C, while for the samples with $MoSi_2$ and carbon and $MoSi_2$ addition it occurs in the temperature range 1200 – 1300°C. Based on results of the dilatometric measurements, temperature of hot pressing of the different samples was established.

Preprints (www.preprints.org) | NOT PEER-REVIEWED | Posted: 26 December 2023 doi:10.20944/preprints202312.1989.v1

3.2. Sintering of TiB_2 with various amounts of carbon

Samples with carbon addition and the reference sample were sintered by hot pressing (HP) at 2100°C. The relative density of the sinters is shown in Figure 3.

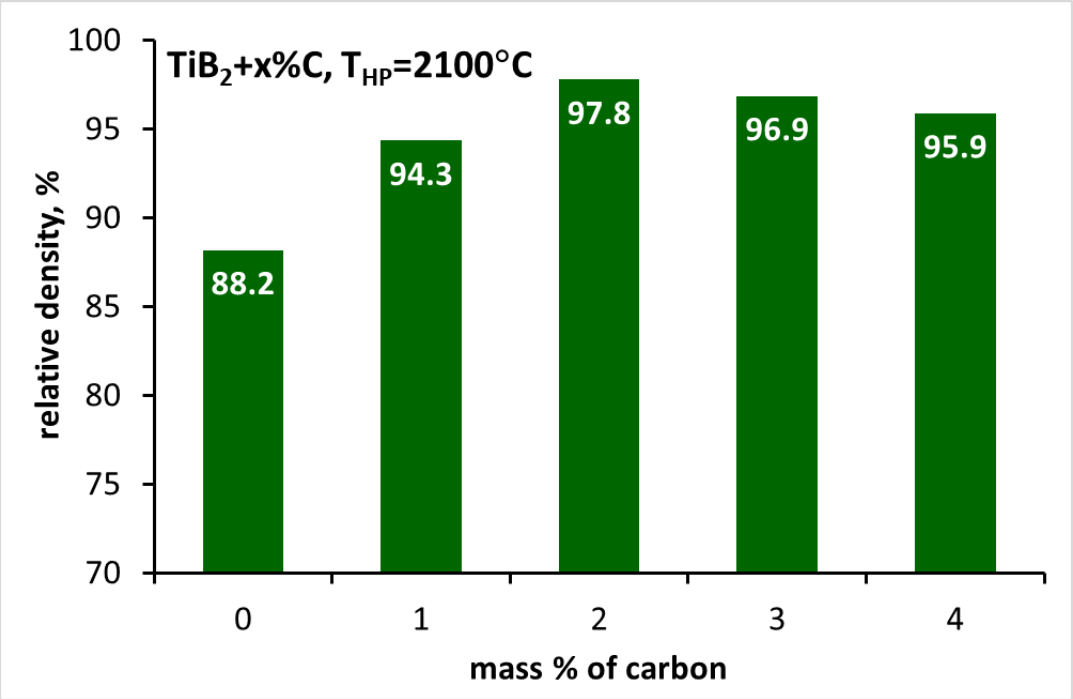

Figure 3. Relative density of the sintered samples containing various amounts of carbon .

The reference sample shows the lowest relative density of 88%, and introduction of 1 wt.% of carbon addition significantly the density (Figure 3). The highest density, around 98%, is achieved by the sinter with 2 wt.% carbon addition, while the density of the sinters with 3 and 4 wt.% carbon additions slightly decreases.

Figure 4 shows SEM microphotographs of the reference sample, which microstructure correlates with the measured density. The sample microstructure is inhomogeneous and significant porosity is visible (black areas).

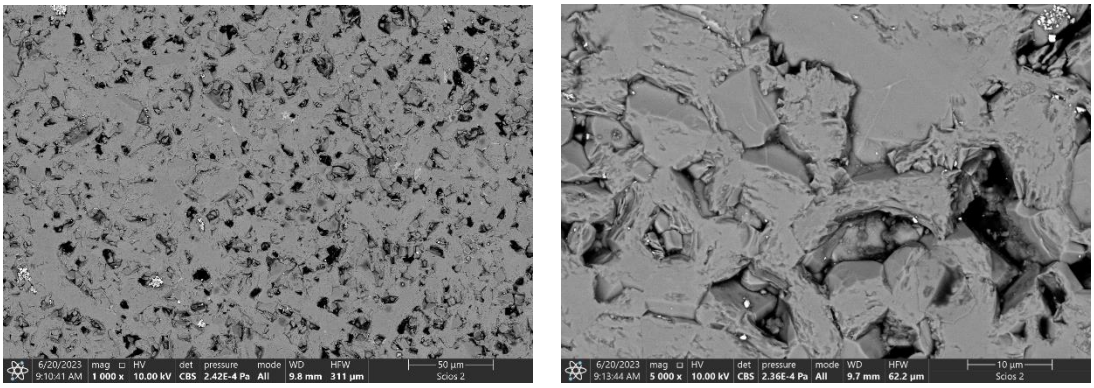

Figure 4. SEM images of the reference TiB_2 sample (TiB2_0).

Preprints (www.preprints.org) | NOT PEER-REVIEWED | Posted: 26 December 2023 doi:10.20944/preprints202312.1989.v1

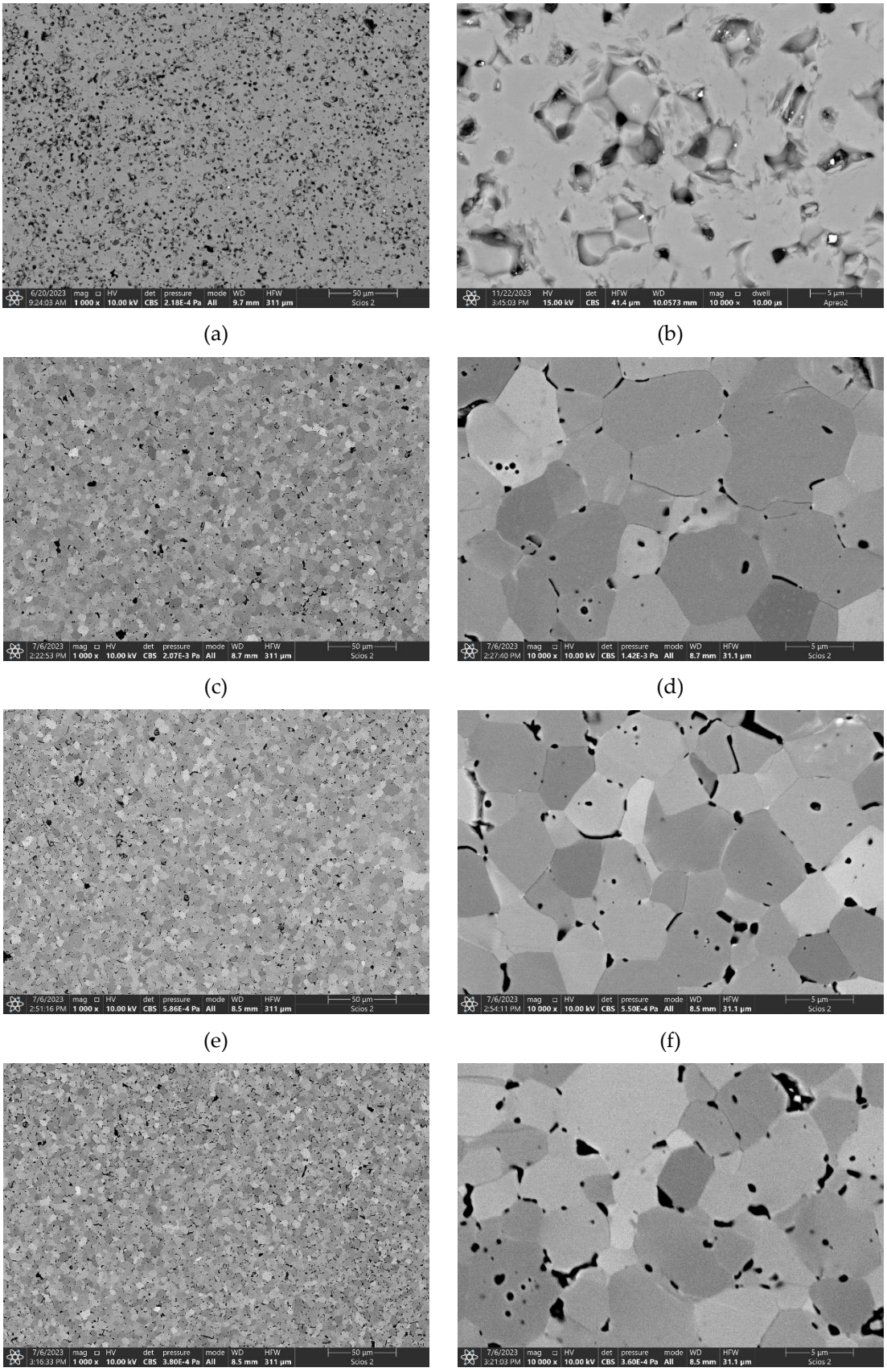

Figure 5. SEM images of TiB_2 samples with carbon addition: a,b) 1 %C; c,d) 2 %C ; e,f) 3 %C ; g,h) 4% C.

Preprints (www.preprints.org) | NOT PEER-REVIEWED | Posted: 26 December 2023 doi:10.20944/preprints202312.1989.v1

Figure 5 shows microstructures of the samples with carbon addition between 1% and 4%. The microstructures are homogeneous and characteristic for dense sinters. Black areas which are visible in the microstructure may be pores but also carbon or carbide inclusions as confirmed by the EDS analysis (Figure 6).

In view of the XRD phase composition analysis, all the obtained polycrystals consist in 100 % of TiB_2. Carbon and carbides may not be detected as their amount in the composites may lay below the detection threshold of the XRD method.

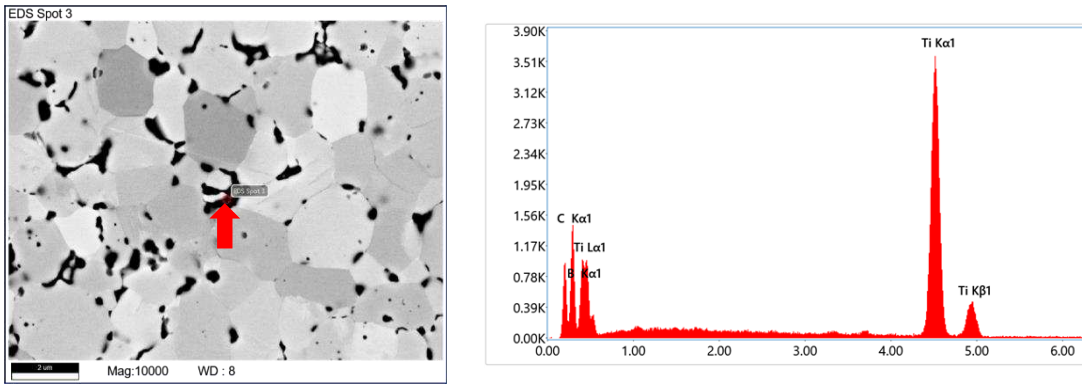

Qualitative analysis, % at.	% B – 54.4	% C – 38.6	% Ti – 7.0

Figure 6. Local chemical composition analysis of the black areas in the TiB_2 sample with 4 wt.% carbon addition .

3.3. Sintering of TiB_2 with various amounts of $MoSi_2$

TiB_2 samples with $MoSi_2$ additive were hot-pressed at 25 MPa at 1800°C. Figure 7 shows dependence of relative density of the sinters on the amount of $MoSi_2$ additive. The lowest density, slightly lower than that of the reference sample, is shown by the composite with 2.5 wt.% $MoSi_2$ addition. A significant increase in density is observed for samples with 5 and 10 wt. % addition of $MoSi_2$. Their relative density is 100 % which clearly indicates good sintering activation of TiB_2 by $MoSi_2$ (Figure 7).

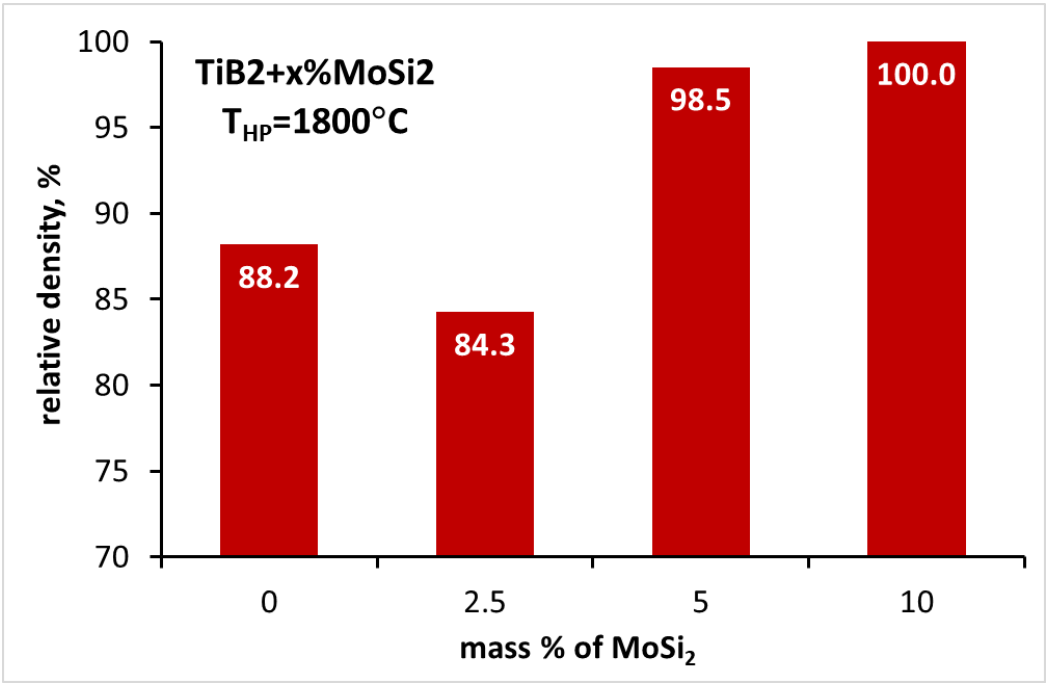

Figure 7. Relative density of the sintered samples containing various amounts of $MoSi_2$.

 doi:10.20944/preprints202312.1989.v1

Figure 8 shows SEM images the TiB_2 composites containing $MoSi_2$. Their microstructures correlate well with the relative density. The highest porosity is found in the sample with the lowest amount i.e.; 2.5 wt.% of $MoSi_2$. The micrographs of the sample clearly show the presence of pores (the darkest areas) (Figs. 8a and 8b). The number of black areas indicating the presence of pores in the samples with 5 and 10 wt.% $MoSi_2$ addition is relatively low (Figures 8c-8f). It can be said that pores are absent in the sample with 5 wt.% $MoSi_2$ addition (Fig. 8f). Based on the XRD phase composition analysis (Table 2), it can be concluded that TiB_2 dominates in all samples. In the samples containing 2.5 wt.% and 5 wt.% $MoSi_2$ also negligible amounts of MoC are identified. In contrast, $MoSi_2$ and MoC can be identified in the sample containing 10 wt.% $MoSi_2$. The presence of molybdenum carbides is a result of a reaction between $MoSi_2$, oxide impurities and carbon from the graphite foil and the graphite die (HP).

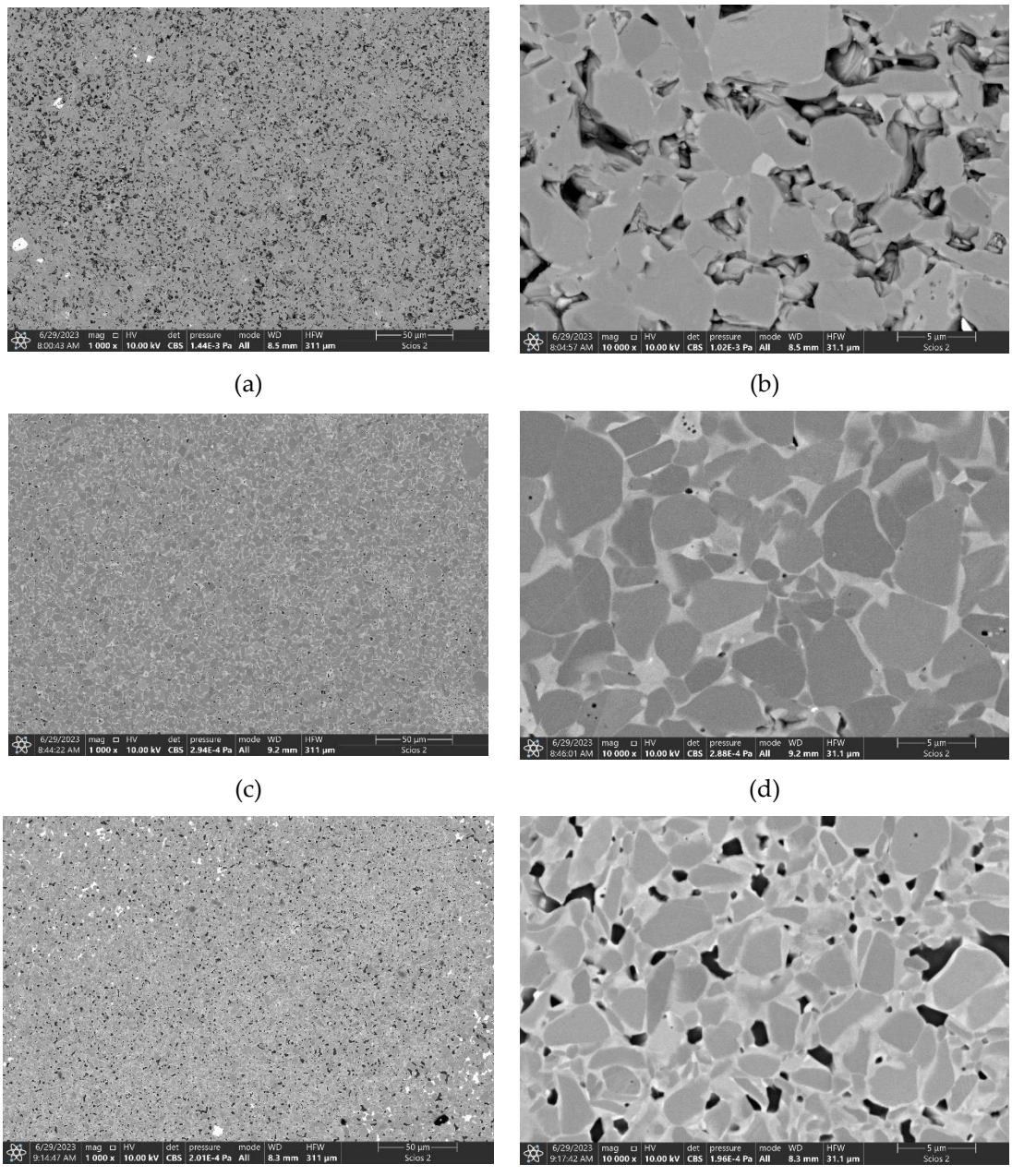

(a) (b) (c) (d) (e) (f)

Figure 8. SEM microphotographs of TiB_2 samples sintered with various amounts of $MoSi_2$ addition: 2.5 wt.%. (a, b); 5.0 wt.%. (c, d) and 10 wt.%. (e, f).

Preprints (www.preprints.org) | NOT PEER-REVIEWED | Posted: 26 December 2023 doi:10.20944/preprints202312.1989.v1

Table 2. Quantitative phase composition of TiB_2+ $MoSi_2$ composites.

Initial phase composition, wt.%	*Phase composition of the HP sinters, wt. %*
97.5% TiB_2, 2.5% $MoSi_2$	68.8% TiB_2 **1**, 29.7% TiB_2 **2**, 1.5% MoC
95% TiB_2, 5.0% $MoSi_2$	69.8% TiB_2 **1**, 28.7% TiB_2 **2**, 1.5% MoC
90% TiB_2, 10% $MoSi_2$	83.0% TiB_2 **1**, 9.4% TiB_2 **2**, 1.0% MoC, 6.6% $MoSi_2$

Furthermore, in the light of the XRD analysis, titanium borides with the same structure but different lattice parameters are present in the composites (Table 3, TiB_2 **1** and TiB_2 **2**).

Table 3. Lattice parameters of titanium boride phases identified in TiB_2+$MoSi_2$ composites.

Lattice parameter, Å	*Theoretical unit cell parameters of TiB_2, [29]*	*TiB_2+2.5% $MoSi_2$*		*TiB_2+5.0% $MoSi_2$*		*TiB_2+10% $MoSi_2$*	
		TiB_2 1	**TiB_2 2**	**TiB_2 1**	**TiB_2 2**	**TiB_2 1**	**TiB_2 2**
a	**3.028**	3.030	3.028	3.030	3.030	3.029	3.029
b	**3.028**	3.030	3.028	3.030	3.030	3.029	3.029
c	**3.228**	3.230	3.230	3.230	3.231	3.231	3.230

The differences in hues of grey visible in the SEM images indicate differences in the chemical composition of individual areas of the samples. Figure 9 shows result of a local chemical composition analysis of the TiB_2 composite containing 10 wt.% $MoSi_2$, and results of the chemical composition analysis are consistent with the results of the phase composition analyses of the sample (Table 2).

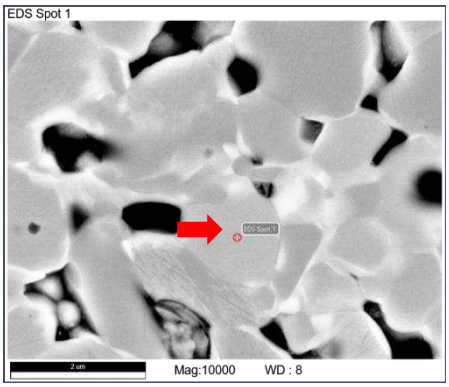

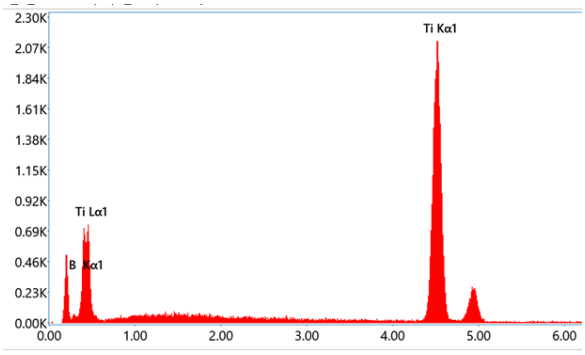

Quantitative analysis, % at.	**% B – 88.3**	**% Ti – 17.7**

(a)

Preprints (www.preprints.org) | NOT PEER-REVIEWED | Posted: 26 December 2023 doi:10.20944/preprints202312.1989.v1

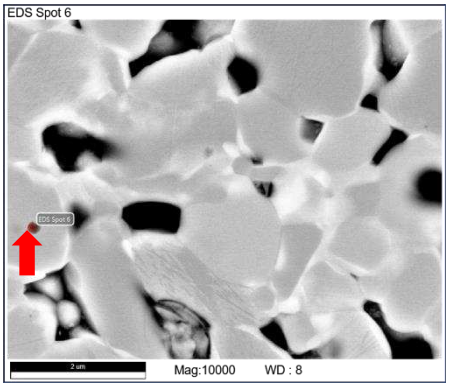

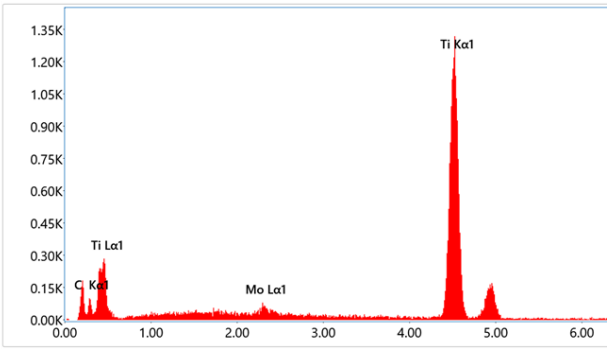

Quantitative analysis, % at.	% Mo – 1.1	% Ti – 80.7	% C – 18.1

(b)

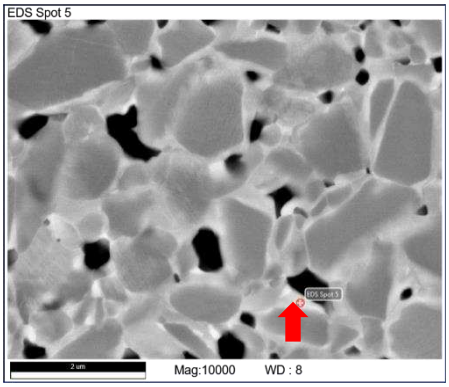

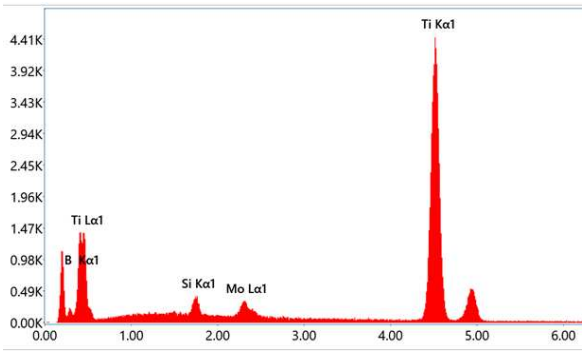

Quantitative analysis, % at.	% B – 34.1	% Mo – 1.5	% Ti – 62.6	% Si – 1.8

(c)

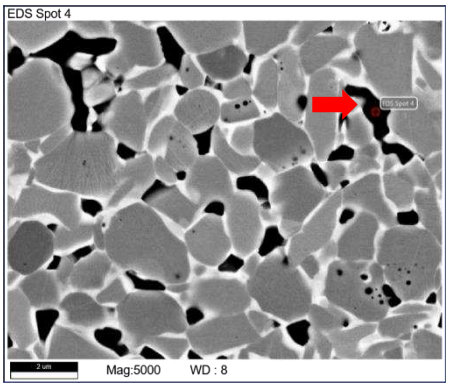

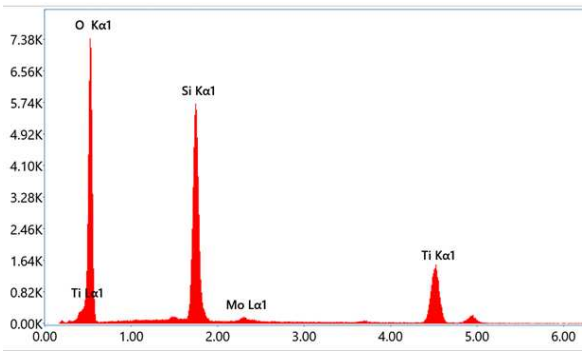

Quantitative analysis, % at.	% O – 74.6	% Mo – 0.4	% Ti – 10.2	% Si – 14.8

(d)

Figure 9. Results of the local chemical composition analysis of TiB_2 with 10 wt.% $MoSi_2$ addition.

In the sinters, grains cores rich in titanium and boron can be identified, which are most likely titanium diboride (Fig. 9a). There are also areas in which in addition to titanium also molybdenum and carbon (Fig. 9b) as well as molybdenum and silicon (Fig. 9c) can be found. Increased amount of molybdenum is identified in light-grey areas around TiB_2 grains (Fig. 9c). There are also the darkest

Preprints (www.preprints.org) | NOT PEER-REVIEWED | Posted: 26 December 2023 doi:10.20944/preprints202312.1989.v1

areas, which in many cases are pores but not always as Figure 9d shows. In many such areas significant amounts of oxygen and silicon can be identified. The reaction between $MoSi_2$ and the oxides which passivate the boride grains can result in the formation of an amorphous phase from the Si-O-B system [30–32].

3.4. Sintering of TiB_2 with 2 wt.% carbon addition and various amounts of $MoSi_2$

TiB_2 samples containing 2 wt.% carbon and different $MoSi_2$ additions were hot-pressed at 1800°C. The relative densities of the resulting polycrystals are shown in Figure 10.

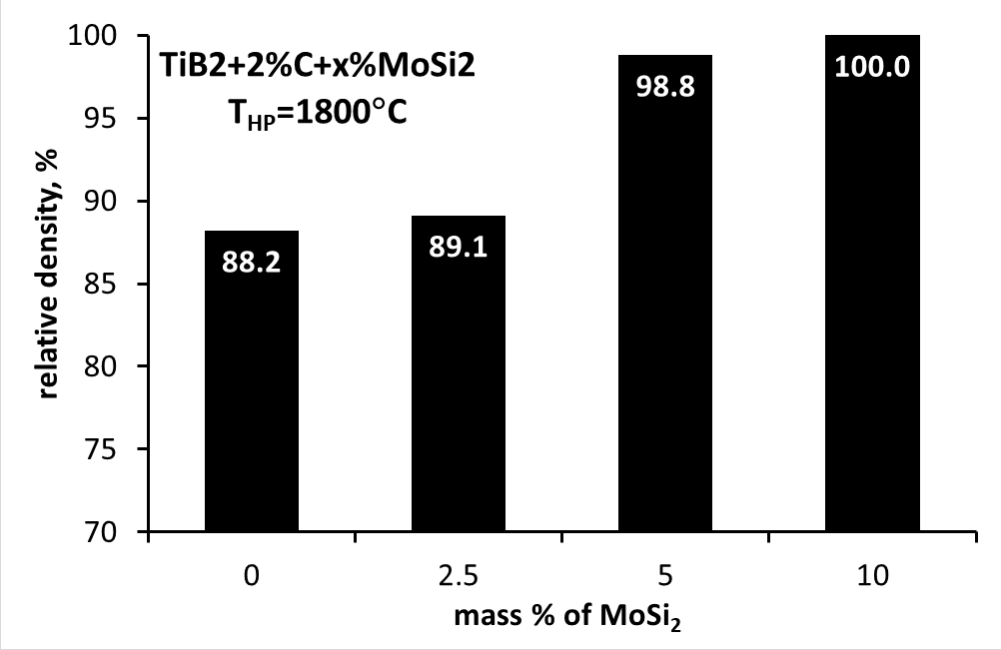

Figure 10. Relative density of sintered samples with 2 wt.% carbon and various amounts of $MoSi_2$.

The lowest density c.a. 90% was exhibited by the sample with the lowest $MoSi_2$ content. An increase in the $MoSi_2$ addition to 5 wt.% led to composites with densities higher than 98 %. The relative density of 100 % was achieved by the composite with the highest $MoSi_2$ addition i.e. 10 wt.% (Fig. 10).

The combination of carbon and $MoSi_2$ additions results in significantly increased density of the composite with 2.5 wt.% $MoSi_2$ addition comparing to the analogous composite without the carbon addition (Figure 7).

Figure 11 shows SEM microstructures of the TiB_2 samples with simultaneous addition of carbon and $MoSi_2$. In the sample with 2.5 wt.% $MoSi_2$ addition, significant porosity is visible (darkest areas). A homogeneous, dense microstructure is presented by samples with 5 and 10 wt.% $MoSi_2$ additions (Fig. 11c-11f). Again, the microstructure of TiB_2 composites with carbon and different amounts of $MoSi_2$ addition is similar to the one typical for cermets i.e. grains consisting of cores and characteristic rims are present (Figure 11).

According to the results of XRD phase composition analysis, the composites after sintering are dominated by titanium boride with different elemental cell sizes (Table 4 and Table 5). The presence of two hexagonal TiB_2 phases (here named TiB_2 1 and TiB_2 2) with different lattice parameters may indicate substitutions within the boride cell by additive-derived elements, i.e. Mo, Si and C. Furthermore, $MoSi_2$ is not present after sintering. It is likely that during sintering, chemical reactions occurred between TiB_2, the oxide impurities i.e. TiO_2 and B_2O_3 and the additives, i.e. $MoSi_2$ and carbon. These reactions resulted in the formation of silicon carbide and complex carbide (Ti, Mo)C_2 (Table 4).

Preprints (www.preprints.org) | NOT PEER-REVIEWED | Posted: 26 December 2023 doi:10.20944/preprints202312.1989.v1

The EDS chemical analysis of the selected sample (TiB2_2C_10MS) is shown in Figure 12. The darkest areas could be pores but also oxide or carbide grains since the areas are rich in oxygen, carbon, silicon and titanium as well as molybdenum. The dark grey areas (cores) are most likely TiB_2 grains, while the light-coloured grain rims, grain boundary areas are rich in molybdenum, titanium, boron and in some places also in carbon.

Table 4. Quantitative phase composition of TiB_2+2%C+x%$MoSi_2$ composites.

Initial phase composition, wt.%	*Phase composition of the HP sinters, wt.%*
95.5% TiB_2, 2.0% C, 2.5% $MoSi_2$	96.8% TiB_2 **1**, 0.1% TiB_2 **2**, 1.7% TiC, 1.4% SiC
95% TiB_2, 2.0% C, 5.0% $MoSi_2$	66.3% TiB_2 **1**, 28.9% TiB_2 **2**, 1.8% SiC, 3.0% (Ti,Mo)C_2
90% TiB_2, 2.0% C, 10% $MoSi_2$	76.1% TiB_2 **1**, 18.6% TiB_2 **2**, 3.1% SiC, 2.2% (Ti,Mo)C_2

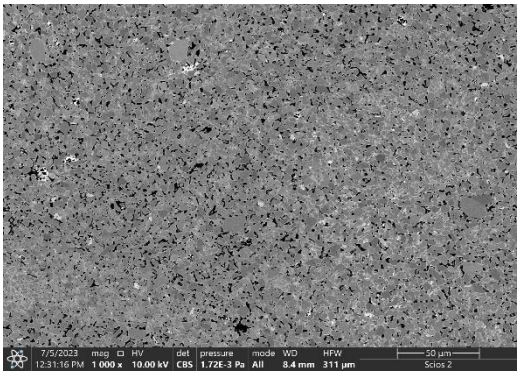

(a)

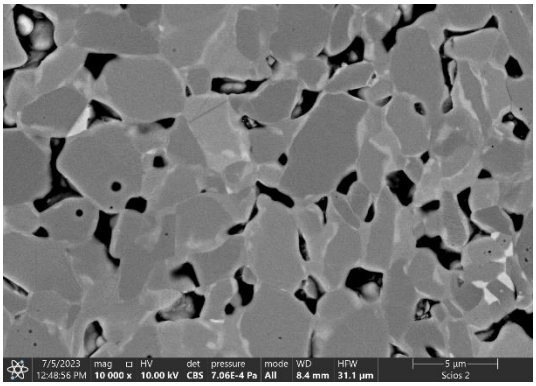

(b)

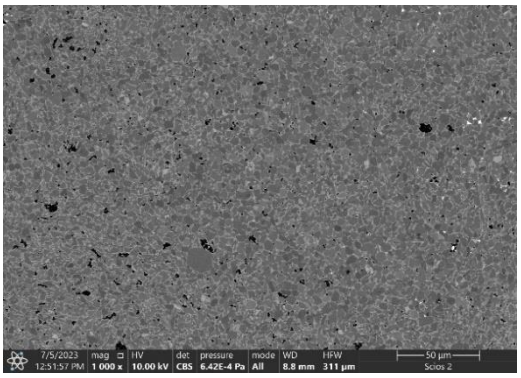

(c)

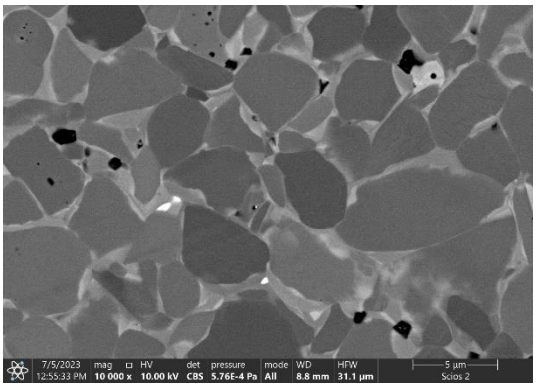

(d)

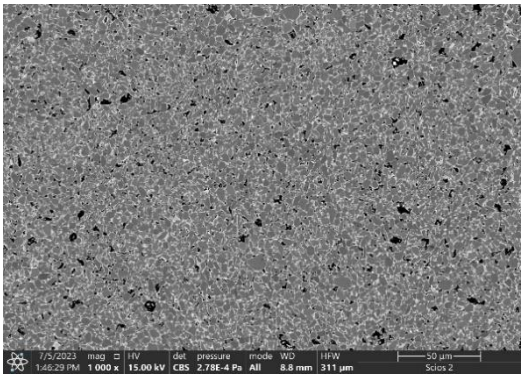

(e)

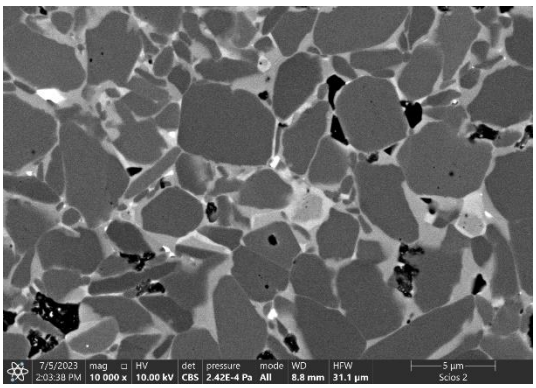

(f)

Preprints (www.preprints.org) | NOT PEER-REVIEWED | Posted: 26 December 2023 doi:10.20944/preprints202312.1989.v1

Figure 11. SEM images of TiB_2 samples with 2% carbon and different amounts of $MoSi_2$ addition: 2.5% (a, b), 5.0% (c, d) and 10% (e, f).

Table 5. Lattice parameters of titanium boride phases identified in TiB_2+2%C+x%$MoSi_2$ composites.

Lattice parameter, Å	*Theoretical unit cell parameters of TiB_2, [29]*	*TiB_2+2%C +2.5% $MoSi_2$*		*TiB_2+2%C +5.0% $MoSi_2$*		*TiB_2+2%C +10% $MoSi_2$*	
		TiB_2 1	**TiB_2 2**	**TiB_2 1**	**TiB_2 2**	**TiB_2 1**	**TiB_2 2**
a	3.028	3.027	3.034	3.029	3.027	3.029	3.027
b	3.028	3.027	3.034	3.029	3.027	3.029	3.027
c	3.228	3.233	3.220	3.230	3.231	3.230	3.232

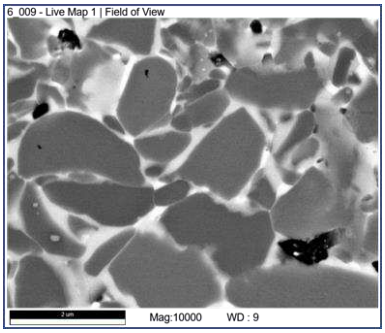

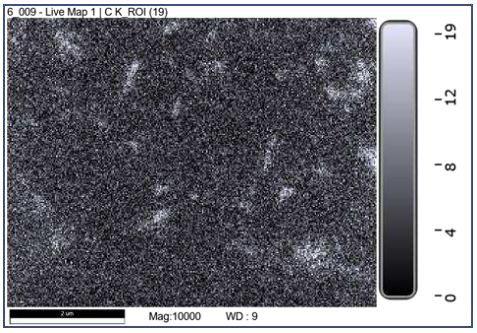

carbon

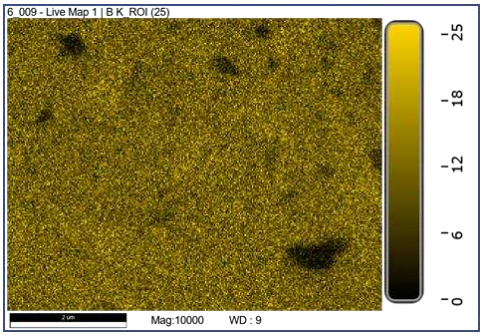

boron

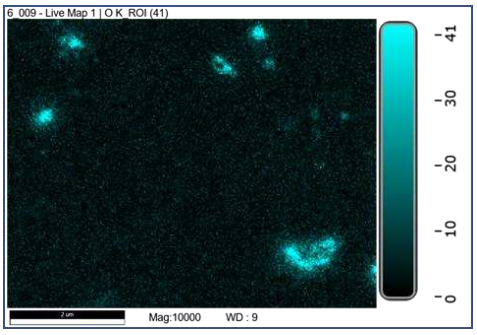

oxygen

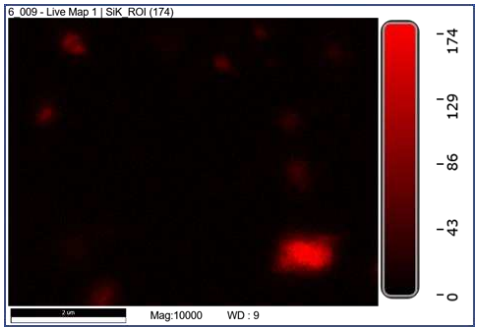

silicon

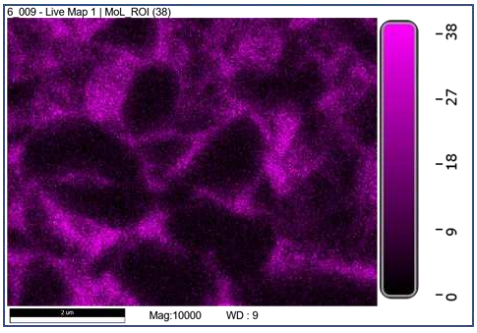

molybdenium

Preprints (www.preprints.org) | NOT PEER-REVIEWED | Posted: 26 December 2023 doi:10.20944/preprints202312.1989.v1

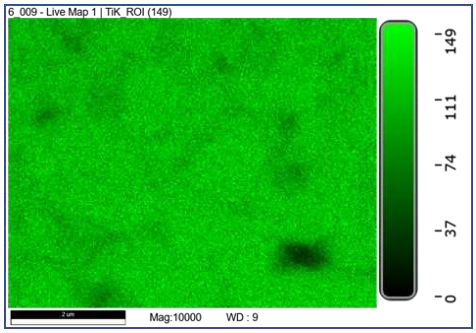

Figure 12. EDS element distribution maps of the TiB_2+2% C+10% $MoSi_2$ composite.

3.5. Mechanical properties of the composites

The composites were tested for Vickers hardness, critical stress intensity factor (K_{Ic}) which is a measure of fracture toughness and Young's modulus. Due to the highly subjective measurement of the critical stress intensity factor using the indentation method, this was carried out on composites with a relative density higher than 95%. The obtained results are summarised in Table 6.

Table 6. Relative density and selected mechanical properties of the composites.

Sample	*Sintering temperature (HP), ℃*	*Relative density, %* *)	*Vickers hardness, GPa*	*K_{IC}, MPa·m$^{0.5}$*	*Young's modulus, GPa*
TiB2_0	2150	88.2±0.3	19.09±6.30	-	-
TiB2_1C	2150	94.3±0.1	26.31±5.86	-	526±12
TiB2_2C	2150	97.8±0.1	25.31±0.77	5.16±0.28	536±9
TiB2_3C	2150	96.9±0.4	23.34±2.17	5.26±0.47	496±16
TiB2_4C	2150	95.9±0.3	25.68±5.29	5.52±0.20	542±10
TiB2_2.5MS	1800	84.3±0.6	16.97±2.86	-	-
TiB2_5.0MS	1800	98.5±0.2	26.21±2.25	6.25±0.51	536±11
TiB2_10MS	1800	100.0±0.4	26.78±3.37	4.86±0.19	504±24
TiB2_2C_2.5MS	1800	89.1±0.8	17.19±1.87	-	440±14
TiB2_2C_5.0MS	1800	98.8±0.4	24.88±2.03	4.79±0.52	543±6
TiB2_2C_10MS	1800	100.0±0.2	24.41±1.90	4.17±0.31	533±12

**) the theoretical density of TiB_2 was 4.52 g/cm^3,*

The hardness of the samples with the lowest densities i.e.; the reference sample (TiB2_0), with 2.5% $MoSi_2$ addition (TiB2_2.5MS) and with 2% carbon and 2.5% $MoSi_2$ addition, is not higher than 20 GPa (Table 6). The introduction of 1% carbon results in a noticeable increase in hardness to 26 GPa. The hardness of composites with 1 to 4% carbon addition is similar and ranges from 23 to 26 GPa. For composites with $MoSi_2$ addition, the lowest hardness is shown by TiB2_2.5MS and TiB2_2C_2.5MS samples. For other composites with $MoSi_2$ addition, the hardness ranges from 24 to 26 GPa.

Based on the measured values of the critical stress intensity factor (Table 6), it can be concluded that the composites exhibit high fracture toughness. The lowest K_{Ic} values, larger than 4 MPa·m$^{0.5}$, are

 doi:10.20944/preprints202312.1989.v1

shown by composites with both additives, i.e. carbon and $MoSi_2$ additives. The K_{Ic} values close to 5 $MPa \cdot m^{0.5}$ are exhibited by composites with carbon additions of 2 to 4%. In contrast, K_{Ic} values between 4.86 and 6.25 $MPa \cdot m^{0.5}$ are shown by composites with $MoSi_2$ additive.

The Young's modulus values of all composites are high, ranging from 496 for the TiB2_3C composite to 543 GPa for the TiB2_2C_5.0MS composite.

4. Results discussion

On the basis of results of the investigations, a favourable effect of all used additives, i.e. carbon, $MoSi_2$ and $MoSi_2$+C, on sinterability of TiB_2 titanium diboride was found. Firstly, a dilatometric sintering analysis was carried out, which showed the validity of the mentioned above sintering activators (Fig. 1 and Fig. 2). Furthermore, it is clear from the dilatometric measurements that the use of 10% $MoSi_2$ addition and the combination of both additives significantly reduces the sintering temperature of TiB_2 (Fig. 2). The sintering temperature of polycrystals with carbon and $MoSi_2$ additives does not exceed 1800°C. For polycrystals with $MoSi_2$, only a 10% addition of molybdenum disilicide reduces the sintering temperature to 1900°C (Fig. 2).

Based on dilatometric sintering analysis, the hot pressing temperatures of all composites were determined. Composites with carbon as well as the reference sample were hot-pressed at 2100°C, while composites with $MoSi_2$ and composites with carbon and $MoSi_2$ were hot-pressed at 1800°C. In many cases, polycrystals with a relative density of 100% were obtained. In the case of carbon addition, the highest densities were obtained when the carbon addition was between 2 and 4 wt.%. Dense polycrystals were produced by adding 5 or 10 wt.% $MoSi_2$ as well as 2 wt.% carbon together with 5 or 10 wt. % $MoSi_2$ (Figs. 3, 7 and 10).

The addition of carbon makes possible to obtain single-phase polycrystals, as evidenced by the phase composition analysis, according to which only TiB_2 is present in such sinters. Also, the microstructures shown in Fig. 5 are characteristic of single-phase and dense sinters when carbon addition is in the range of 2 to 4 wt.%. Phase composition analyses demonstrate the effectiveness of using carbon as an oxide impurity reducer. According to the literature [33], carbon can react both with B_2O_3 and SiO_2 at temperatures close to 1000°C in low vacuum (20 Pa). The local EDS analysis of the chemical composition carried out during SEM observations showed the trace presence of fine particles, whose chemical composition suggests that they may be particles of carbon or boron and titanium carbides (Fig. 6).

The phase composition of the polycrystals sintered with $MoSi_2$ (Table 2) and with carbon and $MoSi_2$ additives shows that composites (Table 4) were obtained in which dominated two TiB_2 phases with different lattice parameters (Tables 3 and 5). In addition, molybdenum carbide was identified in all composites sintered with $MoSi_2$ only, and only the sample with the highest $MoSi_2$ addition showed the presence of this additive. In contrast, for composites with both additives, the dominant are two titanium boride phases with different lattice parameters (Table 5). Silicon and titanium carbides were also identified in these composites, and a complex carbide with the formula $(Mo,Ti)C_2$ was found in samples with 5 and 10 % wt $MoSi_2$ additions. Substitutions of titanium (a_r=140 pm) by Mo (a_r=145 pm), Si (a_r=145 pm) cations as well as boron (a_r=75 pm) by carbon (a_r=70 pm) can led to the presence of hexagonal titanium boride phases with different lattice parameters or in other words to the presence of solid solutions [34]. The presence of $(Mo,Ti,Si)B_2$ solid solutions can be evidenced by a microstructure similar to the one of core-shell cermets. This type of microstructure is often found in composites based on metal borides of the 4th group of the periodic table of chemical elements [21,23,35–37]. SEM micrographs of the TiB2_10.0 composite (Figure 13) show TiB_2 cores and solid-solution shells typical of cermets.

Preprints (www.preprints.org) | NOT PEER-REVIEWED | Posted: 26 December 2023 doi:10.20944/preprints202312.1989.v1

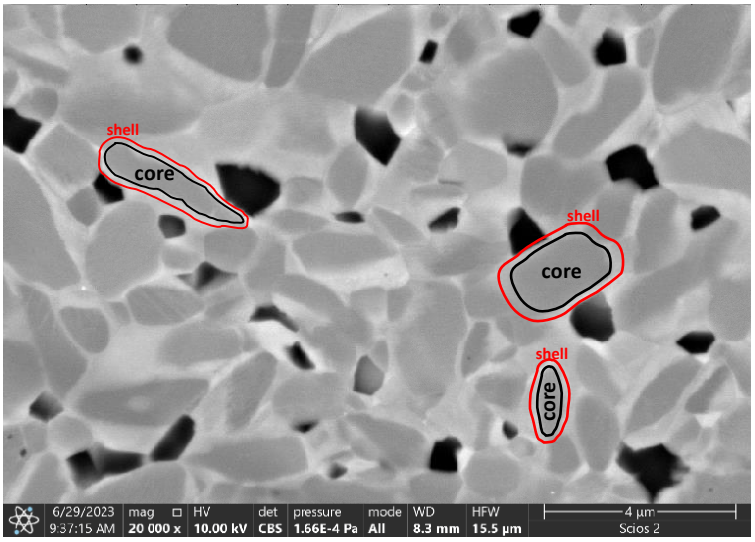

Figure 13. SEM microstructure of the composite with 10 wt.% $MoSi_2$ addition characteristic of cermets.

The EDS chemical element distribution maps made during the SEM observations further showed that in both groups of composites with $MoSi_2$ additive, there are areas enriched in oxygen and silicon (Fig. 9 and Fig. 12). During sintering, a variety of reactions can occur in all composites, including cabothermal reduction of oxides passivating boride particles (Eq.1-2) and reactions between $MoSi_2$ and oxide impurities (Eq.3-5) [4,16,35,38,39], leading to the formation of silica, monoborides and carbides, among others.

$$TiO_2 + 3C \rightarrow TiC + 2CO \uparrow \quad \text{(Eq.1)}$$

$$2B_2O_3 + 7C \rightarrow B_4C + 6CO \uparrow \quad \text{(Eq.2)}$$

$$2MoSi_2 + 2B_2O_3 + TiO_2 \rightarrow TiB_2 + 4SiO_2 + 2MoB \quad \text{(Eq.3)}$$

$$2MoSi_2 + 2B_2O_3 + 2.5C \rightarrow 2.5SiC + 1.5SiO_2 + 2MoB \quad \text{(Eq.4)}$$

$$5MoSi_2 + 7O_2 \rightarrow Mo_5Si_3 + 7SiO_2 \quad \text{(Eq.5)}$$

As it is shown by the composites microstructures in Fig. 8 and Fig. 11, solid solutions can be formed at grain boundaries or, more commonly, at the surface of the boride grains. The literature reports that the formation of the solid solutions in question can be related to the presence of liquid phases with compositions resulting from the initial chemical composition of the composites [4,17,21,36,38,40–42]. The most likely formation of liquid phases is from the Si – B – O system, in which the elements forming the components of the composite can dissolve. It should be added, that in the case of the $MoSi_2$ additive alone, the passivating oxides do not reduce as readily as under the influence of carbon. During cooling, epitaxial precipitation from the liquid phase and the formation of solid solutions can occur [4,17,21,36,42]. The occurrence of the solid solutions discussed, as well as silicide, carbide and SiO_2 phases, may be an indirect evidence of the presence of liquid phases during the sintering of composites with $MoSi_2$ addition. Furthermore, oxygen-rich and silicon-rich particles are identified during the chemical composition analysis, even when $MoSi_2$ and carbon were used as additives (Fig. 12).

According to the literature [30–32], the occurrence of liquid phases from the Si – B – O system is mainly possible in boride composites with silicide additives. These phases can effectively support sintering under pressure by facilitating, among other things, the movement of grains relative to each other [43]. In this case, if the oxides are not fully reduced, even when a small addition of carbon is introduced, it is possible for a reaction between SiO_2 and B_2O_3 to take place resulting in the formation

Preprints (www.preprints.org) | NOT PEER-REVIEWED | Posted: 26 December 2023 doi:10.20944/preprints202312.1989.v1

of a liquid phase from the Si – B – O system, in which elements present in the initial compounds forming the composites can dissolve.

Furthermore, the sintering temperature of composites with $MoSi_2$ is 1800°C and does not exceed the melting point of the silicide (T_m=2050°C) [41,44] but, as reported in the literature [43–46], at temperature higher than 800°C silicides, including molybdenum silicide deform plastically and can fill pores during sintering.

The relationship between density of the composites and the values of the tested mechanical properties is observed. The composites with the highest density, regardless of the additive used, show a high Vickers hardness of 23 to 26 GPa. Also in terms of fracture toughness, all the composites tested show a high value of the critical stress intensity factor K_{Ic} (Table 6). The lowest values of K_{Ic} from 4.18 to 4.79 MPa·$m^{0.5}$ are exhibited by composites with two additives, the fracture toughness of composites with 2 to 4 wt.% carbon addition oscillates around 5 MPa·$m^{0.5}$, while in composites with $MoSi_2$ it ranges from 6.25 to 4.86 MPa·$m^{0.5}$ for 5 wt.% $MoSi_2$ and 10 wt.% $MoSi_2$ addition, respectively. The typical phenomena leading to increase in effective fracture energy are observed in the composites such as intergranular cracking (Figure 14a and Figure 14c), crack deflection as well as crack defragmentation (Fig. 14e and Fig. 14f). It is noteworthy, that the grain boundaries (bonding phase) in composites with 5 wt.% $MoSi_2$ addition are weaker than those in composites with 10 wt.% $MoSi_2$ addition (compare Fig. 14a with Fig. 14b, and Fig. 14c with Fig. 14d). This results in a lower value of the critical stress intensity factor in composites with 10 wt.% $MoSi_2$ addition (Table 6). The fracture then runs predominantly in through the grains as well as along the TiB_2 grain boundaries (Fig. 14b and Fig. 14d).

All high-density composites can be classified as low deformability materials, as evidenced by high values oh their Young's modulus (Table 6).

The values of hardness, fracture toughness and Young's modulus showed by the investigated composites are similar to and often better than those reported in the literature [4,16,38,47].

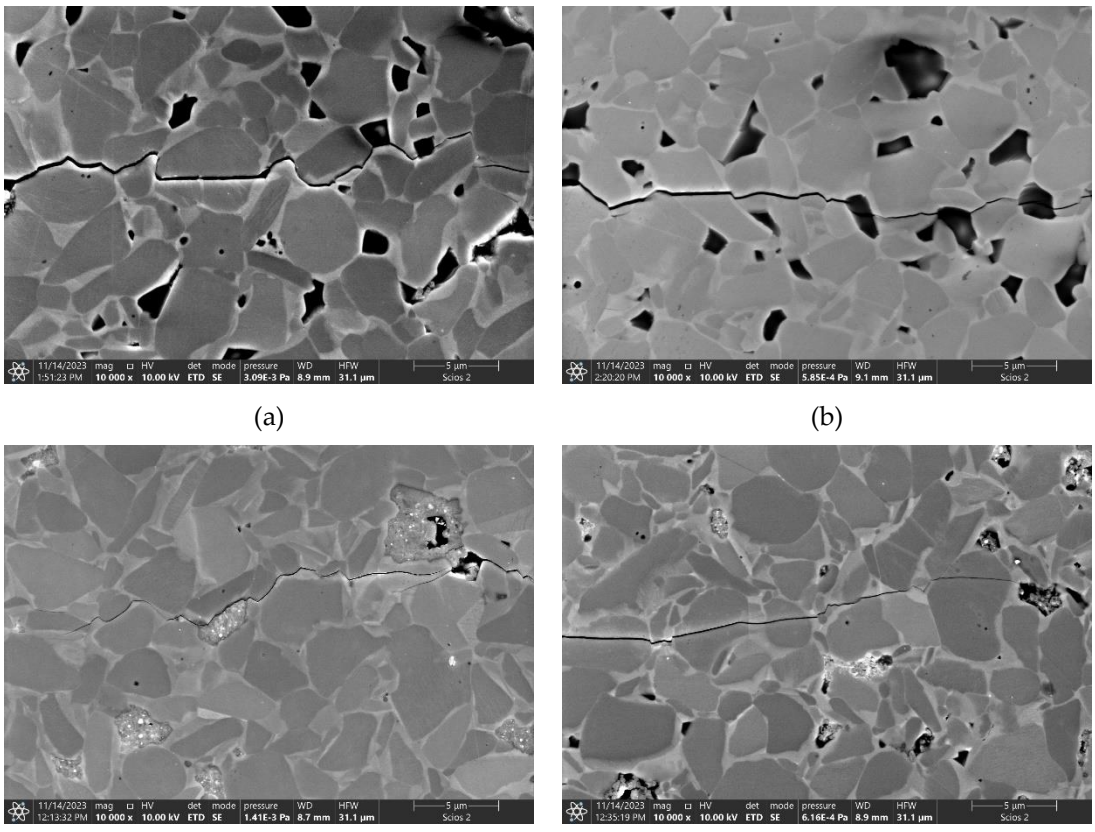

(a) (b)

(c) (d)

 doi:10.20944/preprints202312.1989.v1

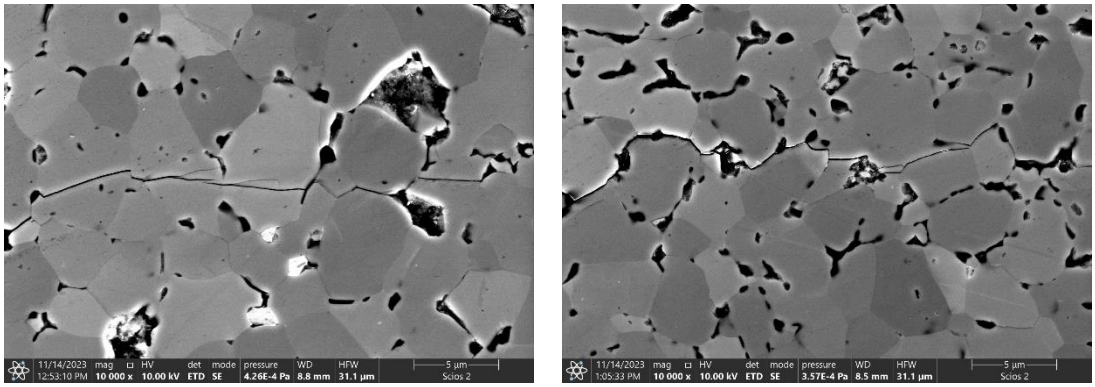

(e) (f)

Figure 14. Course of cracks in composites: a) TiB2_5.0; b) TiB2_10.0; c) TiB2_2C_5.0; d) TiB2_2C_10.0; e) TiB2_3C and f) TiB2_4C.

5. Conclusions

Hot pressing of TiB_2 with carbon, $MoSi_2$ and carbon and $MoSi_2$ additives resulted in single-phase polycrystals and composites with density higher than 95%. Both additives used can be considered as TiB_2 sintering activators. It is noteworthy that the use of $MoSi_2$ as a sintering activating additive significantly reduces the sintering temperature of boride ceramics to 1800°C. With the addition of carbon, it is possible to obtain single-phase polycrystals in which only TiB_2 phase was identified. On the other hand, with the addition of $MoSi_2$ as well as the combined addition of $MoSi_2$ and carbon, it is possible to obtain solid composites with a core-shell microstructure characteristic of cermets. The study shows that carbon is an effective reducer of oxide impurities. It was also found, that due to the liquid phases from the Si – B – O system and the plastic deformation of molybdenum disilicide, it becomes possible to obtain dense composites. The produced materials have potential in high-temperature applications due to their very good properties, i.e. high hardness, high fracture toughness and low deformability. However, further testing of the materials, especially their thermal and chemical properties is required.

Acknowledgements: The work was carried out under the subsidy from the Ministry of Education and Science to the AGH University of Krakow (project no 16.16.160.557). The SEM investigations were supported by the program Excellence Initiative—Research University for the AGH University of Krakow, Grant ID 1449 (PI: M.Ziabka).

References

1. B. Basu, G.B. Raju, A.K. Suri, Processing and properties of monolithic TiB_2 based materials, Int. Mater. Rev. 51 (2006) 352–374. doi:10.1179/174328006X102529.
2. B.R. Golla, A. Mukhopadhyay, B. Basu, S.K. Thimmappa, Review on ultra-high temperature boride ceramics, Prog. Mater. Sci. 111 (2020) 100651. doi:10.1016/j.pmatsci.2020.100651.
3. W.G. Fahrenholtz, G.E. Hilmas, Ultra-high temperature ceramics: Materials for extreme environments, Scr. Mater. 129 (2017) 94–99. doi:10.1016/j.scriptamat.2016.10.018.
4. T.S.R.C. Murthy, B. Basu, R. Balasubramaniam, A.K. Suri, C. Subramanian, R.K. Fotedar, Processing and Properties of TiB_2 with $MoSi_2$ Sinter-additive: A First Report, J. Am. Ceram. Soc. 89 (2006) 131–138. doi:10.1111/j.1551-2916.2005.00652.x.
5. F. Monteverde, A. Bellosi, Efficacy of HfN as sintering aid in the manufacture of ultrahigh-temperature metal diborides-matrix ceramics, J. Mater. Res. 19 (2004) 3576–3585. doi:10.1557/JMR.2004.0460.
6. F. Monteverde, A. Bellosi, Beneficial Effects of AlN as Sintering Aid on Microstructure and Mechanical Properties of Hot-pressed ZrB_2, Adv. Eng. Mater. 5 (2003) 508–512. doi:10.1002/adem.200300349.
7. F. Monteverde, A. Bellosi, Effect of the addition of silicon nitride on sintering behaviour and microstructure of zirconium diboride, Scr. Mater. 46 (2002) 223–228. doi:10.1016/S1359-6462(01)01229-5.
8. L.-H. Li, H.-E. Kim, E. Son Kang, Sintering and mechanical properties of titanium diboride with aluminum nitride as a sintering aid, J. Eur. Ceram. Soc. 22 (2002) 973–977. doi:10.1016/S0955-2219(01)00403-4.

9. J.-H. Park, Y.-H. Koh, H.-E. Kim, C.S. Hwang, E.S. Kang, Densification and Mechanical Properties of Titanium Diboride with Silicon Nitride as a Sintering Aid, J. Am. Ceram. Soc. 82 (2004) 3037–3042. doi:10.1111/j.1151-2916.1999.tb02199.x.
10. S.K. Bhaumik, C. Divakar, A.K. Singh, G.S. Upadhyaya, Synthesis and sintering of TiB_2 and TiB_2–TiC composite under high pressure, Mater. Sci. Eng. A 279 (2000) 275–281. doi:10.1016/S0921-5093(99)00217-8.
11. E.S. Kang, C.H. Kim, Improvements in Mechanical Properties of TiB_2 by the Dispersion of B_4C Particles, J. Mater. Sci. 4 (1989) 580.
12. E.S. Kang, C.W. Jang, C.H. Lee, C.H. Kim, D.K. Kim, Effect of Iron and Boron Carbide on the Densification and Mechanical Properties of Titanium Diboride Ceramics, J. Am. Ceram. Soc. 72 (1989) 1868–1872. doi:10.1111/j.1151-2916.1989.tb05993.x.
13. F. Rodríguez-Rojas, V. Zamora, F. Guiberteau, A.L. Ortiz, Solid-state spark plasma sintering of super wear resistant B_4C–SiC–TiB_2 triplex-particulate composites, Ceram. Int. 49 (2023) 5532–5537. doi:10.1016/j.ceramint.2022.11.181.
14. S. Torizuka, K. Sato, J. Harada, H. Yamamoto, H. Nishio, Microstructure and Sintering Mechanism of TiB2–ZrO2–SiC Composite, J. Ceram. Soc. Jpn. 100 (1992) 392–397.
15. S. Torizuka, K. Sato, H. Nishio, T. Kishi, Effect of SiC on Interfacial Reaction and Sintering Mechanism of TiB_2, J. Am. Ceram. Soc. 78 (1995) 1606–1610. doi:10.1111/j.1151-2916.1995.tb08858.x.
16. A. Mukhopadhyay, G.B. Raju, B. Basu, Understanding Influence of $MoSi_2$ Addition (5 Weight Percent) on Tribological Properties of TiB_2, Metall. Mater. Trans. A 39 (2008) 2998–3013. doi:10.1007/s11661-008-9652-9.
17. T.S.R.C. Murthy, R. Balasubramaniam, B. Basu, A.K. Suri, M.N. Mungole, Oxidation of monolithic TiB_2 and TiB_2–20wt.% $MoSi_2$ composite at 850°C, J. Eur. Ceram. Soc. 26 (2006) 187–192. doi:10.1016/j.jeurceramsoc.2004.10.025.
18. T.S.R.C. Murthy, J.K. Sonber, C. Subramanian, R.K. Fotedar, S. Kumar, M.R. Gonal, A.K. Suri, A new TiB_2+$CrSi_2$ composite – Densification, characterization and oxidation studies, Int. J. Refract. Met. Hard Mater. 28 (2010) 529–540. doi:10.1016/j.ijrmhm.2010.02.012.
19. G.B. Raju, B. Basu, Densification, Sintering Reactions, and Properties of Titanium Diboride With Titanium Disilicide as a Sintering Aid, J. Am. Ceram. Soc. 90 (2007) 3415–3423. doi:10.1111/j.1551-2916.2007.01911.x.
20. G.B. Raju, A. Mukhopadhyay, K. Biswas, B. Basu, Densification and high-temperature mechanical properties of hot pressed TiB_2–(0–10wt.%) $MoSi_2$ composites, Scr. Mater. 61 (2009) 674–677. doi:10.1016/j.scriptamat.2009.05.031.
21. L. Silvestroni, H.-J. Kleebe, S. Lauterbach, M. Müller, D. Sciti, Transmission electron microscopy on Zr- and Hf-borides with $MoSi_2$ addition: Densification mechanisms, J. Mater. Res. 25 (2010) 828–834. doi:10.1557/JMR.2010.0126.
22. D. Sciti, L. Silvestroni, G. Celotti, C. Melandri, S. Guicciardi, Sintering and Mechanical Properties of ZrB_2 -$TaSi_2$ and HfB_2 -$TaSi_2$ Ceramic Composites, J. Am. Ceram. Soc. 91 (2008) 3285–3291. doi:10.1111/j.1551-2916.2008.02593.x.
23. L. Silvestroni, D. Sciti, Densification of ZrB_2-$TaSi_2$ and HfB_2-$TaSi_2$ Ultra-High-Temperature Ceramic Composites, J. Am. Ceram. Soc. 94 (2011) 1920–1930. doi:10.1111/j.1551-2916.2010.04317.x.
24. T. Watanahe, K. Shoubu, Mechanical Properties of Hot-Pressed TiB_2-ZrO_2 Composites, J. Am. Ceram. Soc. 68 (1985) C-34-C–36. doi:10.1111/j.1151-2916.1985.tb15273.x.
25. R. Telle, S. Meyer, G. Petzow, E.D. Franz, Sintering behaviour and phase reactions of TiB_2 with ZrO2 additives, Mater. Sci. Eng. A 105–106 (1988) 125–129. doi:10.1016/0025-5416(88)90488-0.
26. J. Schneider, K.H. Zum Gahr, R. Müller, E.. Franz, Einfluß des ZrO_2-Zusatzes auf mechanische Eigenschaften und den ungeschmierten Gleitverschleiß von TiB_2-ZrO_2-Mischkeramiken, Materwissenchaft Und Werkstofftechnik 27 (1996) 359–366.
27. Y. Muraoka, M. Yoshinaka, K. Hirota, O. Yamaguchi, Hot isostatic pressing of TiB_2-ZrO_2(2 mol% Y2O3) composite powders, Mater. Res. Bull. 31 (1996) 787–792. doi:10.1016/0025-5408(96)00069-4.
28. T. Graziani, A. Bellosi, Sintering and Characterization of TiB_2 -B_4C-ZrO_2 Composites, Mater. Manuf. Process. 9 (1994) 767–780. doi:10.1080/10426919408934945.
29. ICSD 98-003-0330 Titanium Boride, (n.d.).
30. M. Singh, H. Wiedemeier, Chemical Interactions in Diboride-Reinforced Oxide-Matrix Composites, J. Am. Ceram. Soc. 74 (1991) 724–727. doi:10.1111/j.1151-2916.1991.tb06915.x.
31. G.J.K. Harrington, G.E. Hilmas, W.G. Fahrenholtz, Effect of Carbon and Oxygen on the Densification and Microstructure of Hot Pressed Zirconium Diboride, J. Am. Ceram. Soc. 96 (2013) 3622–3630. doi:10.1111/jace.12561.
32. S. Baik, P.F. Becher, Effect of Oxygen Contamination on Densification of TiB_2, J. Am. Ceram. Soc. 70 (1987) 527–530. doi:10.1111/j.1151-2916.1987.tb05699.x.
33. Y. Yan, Z. Huang, S. Dong, D. Jiang, Pressureless Sintering of High-Density ZrB_2 ?SiC Ceramic Composites, J. Am. Ceram. Soc. 89 (2006) 3589–3592. doi:10.1111/j.1551-2916.2006.01270.x.
34. 8.2: Atomic and Ionic Radius, (n.d.). https://chem.libretexts.org/@go/page/98634?pdf.

35. T.R. Paul, M.K. Mondal, M. Mallik, Densification behavior of ZrB_2–$MoSi_2$–SiCw composite processed by multi stage spark plasma sintering, Ceram. Int. 47 (2021) 31948–31972. doi:10.1016/j.ceramint.2021.08.081.
36. F. Monteverde, R.J. Grohsmeyer, A.D. Stanfield, G.E. Hilmas, W.G. Fahrenholtz, Densification behavior of ZrB_2-$MoSi_2$ ceramics: The formation and evolution of core-shell solid solution structures, J. Alloys Compd. 779 (2019) 950–961. doi:10.1016/j.jallcom.2018.11.238.
37. D. Sciti, F. Monteverde, S. Guicciardi, G. Pezzotti, A. Bellosi, Microstructure and mechanical properties of ZrB_2–$MoSi_2$ ceramic composites produced by different sintering techniques, Mater. Sci. Eng. A 434 (2006) 303–309. doi:10.1016/j.msea.2006.06.112.
38. A. Rabiezadeh, A.M. Hadian, A. Ataie, Synthesis and sintering of TiB_2 nanoparticles, Ceram. Int. 40 (2014) 15775–15782. doi:10.1016/j.ceramint.2014.07.102.
39. M. Mashhadia, M. Shambulia, S. Safib, Effect of $MoSi_2$ addition and particle size of SiC on pressureless sintering behavior and mechanical properties of ZrB_2–SiC–$MoSi_2$ composites, J. Mater. Res. Technol. 5 (2016) 200–205. doi:10.1016/j.jmrt.2015.10.003
40. L. Silvestroni, S. Failla, I. Neshpor, O. Grigoriev, Method to improve the oxidation resistance of ZrB_2 -based ceramics for reusable space systems, J. Eur. Ceram. Soc. 38 (2018) 2467–2476. doi:10.1016/j.jeurceramsoc.2018.01.025.
41. A. Suri, N. Krishnamurthy, C. Subramanian, Issues in the synthesis and fabrication of refractory carbides, borides, silicides and their mixtures, in: T. Ohji, M. Singh (Eds.), Process. Manuf. Technol. Struct. Multifunct. Mater., John Wiley & Sons, Inc., Hoboken, New Jersey, 2000: pp. 69–79.
42. T. Dasgupta, J. Etourneau, B. Chevalier, S.F. Matar, A.M. Umarji, Structural, thermal, and electrical properties of $CrSi_2$, J. Appl. Phys. 103 (2008). doi:10.1063/1.2917347.
43. R. Rosenkranz, G. Frommeyer, Microstructures and Properties of the Refractory Compounds $TiSi_2$ and $ZrSi_2$, Int. J. Mater. Res. 83 (1992) 685–689. doi:10.1515/ijmr-1992-830909.
44. Y. Jeng, E.J. Lavernia, Processing of molybdenum disilicide, J. Mater. Sci. 29 (1994) 2557–2571.
45. T. Nakano, K. Hagihara, Y. Nakai, Y. Umakoshi, Plastic deformation behavior of $NbSi_2$/$MoSi_2$ crystals with oriented lamellae, Intermetallics 14 (2006) 1345–1350. doi:10.1016/j.intermet.2005.10.017.
46. H. Inui, M. Moriwaki, S. Ando, M. Yamaguchi, Plastic deformation of single crystals of $CrSi_2$ with the C_{40} structure, Mater. Sci. Eng. A 239–240 (1997) 63–68. doi:10.1016/S0921-5093(97)00561-3.
47. Z. Fu, R. Koc, Microstructure and mechanical properties of hot pressed submicron TiB_2 powders, Ceram. Int. 44 (2018) 9995–9999. doi:10.1016/j.ceramint.2018.02.153.